Supporting Information

Crystallization manipulation and holistic defect passivation toward stable and efficient inverted perovskite solar cells

Cong Zhang[1#], Haiyun Li[1#], Cheng Gong[1], Qixin Zhuang[1], Jiangzhao Chen[1*], Zhigang Zang[1*]

[1]Key Laboratory of Optoelectronic Technology & Systems (Ministry of Education), Chongqing University, Chongqing 400044, China

[#]The authors contributed equally to this work.

*Correspondence to: jiangzhaochen@cqu.edu.cn (J.C.); zangzg@cqu.edu.cn (Z.Z.)

Methods

Materials

All chemicals and solvents were used as received without further purification. The nickel nitrate hexahydrate ($Ni(NO_3)_2 \cdot 6H_2O$, 99.999%), sodium hydroxide (NaOH,99.9%), *N,N*-dimethylformamide (DMF, 99.8%), dimethyl sulfoxide (DMSO, 99.8%), chlorobenzene (CB, 99.8%), isopropanol (IPA, 99.5%) and Al_2O_3 dispersed solution (20 wt.% in IPA) were all purchased from Sigma Aldrich. Methylammonium bromide (MABr, 99.9%), methylammonium iodide (MAI, 99.9%), formamidium iodide (FAI, 99.9%), cesium iodide (CsI, 99.999%), lead (II) iodide (PbI_2 ultra-dry, 99.999% purity), and lead (II) bromide ($PbBr_2$, 99.99%) were purchased from Advanced Election Technology CO., Ltd. Poly(triaryl amine) (PTAA, molecular weight distribution: 6000–15000) and bathocuproine (BCP) were purchased from Xi'an Polymer Light Technology Corp. Phenformin hydrochloride (PFCl, 97%) was bought from Aladdin Biochem Technology Corp. S-methylisothiosemicarbazide hydroiodide (SMI, 98%) was bought from Macklin Inc. NiO_x nanoparticles (NPs) were synthesized according to the previous work[1].

Preparation of perovskite precursor solution

For $FA_{0.95}Cs_{0.05}PbI_3$ double-cation perovskite films, 1.4 M perovskite precursor solution was prepared through dissolving 228.4 mg FAI, 18.2 mg CsI, and 645.4 mg PbI_2 in mixed solvents of DMF and DMSO (v/v, 4/1).

For $(FA_{0.85}MA_{0.15})_{0.95}Cs_{0.05}Pb(I_{0.85}Br_{0.15})_3$ triple-cation perovskite films, 1.5 M perovskite precursor solution was prepared by mixing CsI, FAI, MABr, PbI_2 and $PbBr_2$ in 1 ml mixed solvents of DMF: DMSO (v/v, 4/1), where excess 5 mol% of PbI_2 was added to improve the device performance.

Device fabrication

The patterned indium tin oxides (ITO) was ultrasonically cleaned with detergent, deionized water, and ethanol for 20 min each. After ultraviolet-ozone (UVO) treatment for 20 min, the 20 mg/ml NiO_x NPs aqueous solution was spin-coated on substrates at 5000 rpm for 30 s in air, followed by annealing at 150 °C for 10 min. And then, obtained NiO_x films were immediately transferred into the glove box filled with nitrogen. 1 mg/ml PTAA solution in CB was spin-coated onto NiO_x films at 6000 rpm for 30 s. After that, Al_2O_3 dispersion solution (0.4 wt% in IPA) was spin-coated on PTAA films at 5000 rpm for 30 s.

For the double-cation perovskite films, $FA_{0.95}Cs_{0.05}PbI_3$ perovskite precursor solutions without and with PFCl were spin-coated on glass/ITO/NiO_x/PTAA/Al_2O_3 substrate at 2000 rpm for 10 s and then at 4000 rpm for 40 s. During the second spin coating step, 150 μL CB was dropped onto the perovskite film at 6 s before ending the program. The perovskite sample was annealed at 100 °C for 30 min.

For the triple-cation perovskite films, $(FA_{0.85}MA_{0.15})_{0.95}Cs_{0.05}Pb(I_{0.85}Br_{0.15})_3$ precursor solutions without and with PFCl were spin-coated onto glass/ITO/NiO_x/PTAA/Al_2O_3 substrate at 1000 rpm for 10 s and then at 5000 rpm for 20 s. 200 μL CB was slowly dripped onto the center of the film at 5 s before the end of spin-coating. The as-prepared perovskite films were subsequently annealed on a hotplate at 100 ℃ for 60 min.

For the double- and triple-cation perovskite films with surface modification, different concentrations of SMI solutions (0.5, 1 and 2 mg/ml) in IPA were dynamically spin-coated on the perovskite surface at 5000 rpm for 30 s, followed by annealing at 100 ℃ for 1 min.

Subsequently, the 23 mg/ml of $PC_{61}BM$ solution in CB was spin-coated on the perovskite films at 2500 rpm for 40 s. Afterward, the 5 mg/ml of BCP super-saturated solution in IPA was filtered and then spin-coated on $PC_{61}BM$ film at 5000 rpm for 30 s. Finally, a 100 nm Ag electrode was deposited by thermal evaporation.

Characterization of the solar cells

The current density–voltage (*J-V*) characteristics of the devices were measured by an AM 1.5G solar simulator equipped with 450 W Xenon lamp (Newport, 2612A) and a Keithley 2400 source meter. Light intensity was adjusted to AM 1.5G one sun (100 mW/cm^2) with a NIM calibrated standard Si solar cell. *J–V* curves were measured in forward scan (from –0.1 to 1.2 V) and reverse scan (from 1.2 to –0.1 V). The active area of PSCs was defined to be 0.09 cm^2 by a black metal mask. For incident photon-to-current conversion efficiency (IPCE) measurement, a Newport Instruments system (Newport-74125) coupled with a lock-in amplifier and a 300 W Xenon lamp was employed. Transient photocurrent and photovoltage measurements were performed using a system excited by a 532 nm (1000 Hz, 6 ns) pulsed laser. Recording photocurrent or photovoltage decay process used a 1 GHz Agilent digital oscilloscope (DSO-X3102A) with a 50 X or 1 MX sampling resistor.

Characterization of the device stability

The ambient stability measurement of the encapsulated devices was conducted at 20~30 RH in the

dried-air glove box for 2976 h. The light stability measurement of the unencapsulated devices was conducted under a continuous one-sun illumination (a light-emitting diode lamp without UV filter) in a N_2-filled glove box for 1008 h. The thermal stability measurement of the encapsulated devices was conducted at 85 °C in N_2 for 864 h. As for *J-V* characterization, the PSCs were measured by an AM 1.5G solar simulator equipped with 450 W Xenon lamp (Newport, 2612A) and a Keithley 2400 source meter (scan rate was 0.1 V s^{-1}) at different time intervals.

Characterization of perovskite films

The X-ray diffraction patterns were acquired using a Rigaku Ultima IV equipped with Cu Kα radiation (λ = 1.5406 Å). The UV-vis absorption spectra of perovskite films were measured by using Shimadzu UV3600 Spectrophotometer. The Fourier transform infrared spectroscopy (FTIR spectra) were collected in the transmittance mode on the Nicolet iS50 Infrared Fourier spectrometer instrument. X-ray photoelectron spectroscopy (XPS) measurements were conducted on Thermo Fisher Escalab 250Xi spectrometer by using a monochromatized Al Kα source (1486.6 eV). XPS was calibrated using the peak position of C1s. The steady-state PL spectra were recorded by a fluorescence spectrometer (FLS1000, Edinburgh Instruments Ltd.) using 380 nm or 550 nm excitation light source. time resolved photoluminescence (TRPL) spectra were collected by a fluorescence spectrophotometer (FLS1000, Edinburgh Instruments Ltd.) with the excitation of a 380 nm laser pulsed. The change of light absorption during spin-coating of perovskite film was studied by self-made in-situ light absorption equipment. The field emission scanning electron microscopy (FEI Inspect F50) was employed to characterize the cross-sectional and surface morphology of perovskite films. High resolution transmission electron microscope (HRTEM) images were performed on the FEI Talos F200S (performed at 200 kV) instrument. The thin-film samples were scrape off with a knife and dissolved by chlorobenzene in vials. After ultrasonic dispersion, the droplets were dried on the copper net to provide the sample for HRTEM.

ToF-SIMS measurements

The ToF-SIMS measurements (Model TOF-SIMS V, ION-TOF GmbH) were performed with the pulsed primary ions from an oxygen-ion beam (1 keV) for the sputtering and a Bi^+ pulsed primary ion beam for the analysis (25 keV).

^{1}H NMR spectra measurements

^{1}H NMR spectra were collected on a Bruker Advanced III 400 MHz spectrometer. The samples

were dissolved by DMSO-d6 in vials to provide the sample solution for NMR.

TRMC measurements

For time-resolved microwave conductivity (TRMC) measurements, the perovskite film samples were deposited on glass and excited with a fast nanosecond laser pulse (LO-TIS TII Nd:YAG Laser System LS-2145-OPO), which generated a certain amount of carriers within the samples. Subsequently, we probed the samples with a microwave and the reflected microwave intensity was monitored as a function of time following photo-excitation with a microwave analyzer (N9915A FieldFox, Keysight). To enhance the sensitivity, we introduced a high-Q microwave cavity, which has a resonance frequency of ~4.3 GHz. The source power of the microwave was set at 1 mW, and the excitation laser wavelength was 530 nm with a pulse length of ~5 ns.

Grazing incidence X-ray diffraction

The samples were measured by grazing incidence X-ray diffraction (GIXRD) instrument (Empyrean) with 40 kV, 40 mA radiation (Cu Kα, l = 0.15406 nm, scan speed =0.02°/min). The scan range were 13.5° to 14.5° in the 2θ range. The incident angle (ω) was 0.3°, 0.5°, 0.7°, 0.9°, 1.1° and 1.3°. The interplanar crystal spacing (d-spacing) was calculated by the Bragg equation of $n\lambda = 2d\sin\theta$. The increased interplanar crystal spacing responds to the lattice expansion.

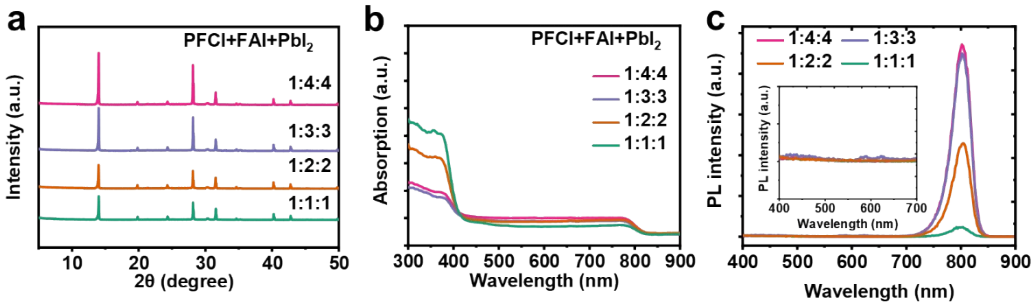

Fig. S1. a XRD, **b** UV-vis and **c** PL spectra of the perovskite films with different mole ratios of PFCl, FAI and PbI_2. 1 M precursor solution was prepared through dissolving different ratios of PFCl, FAI, and PbI_2 (1:1:1, 1:2:2, 1:3:3 and 1:4:4) in mixed DMF and DMSO (v/v, 4/1). The perovskite films were prepared by spin-coating as-prepared precursor solutions on glass substrates and annealing at 100 ℃ for 30 min.

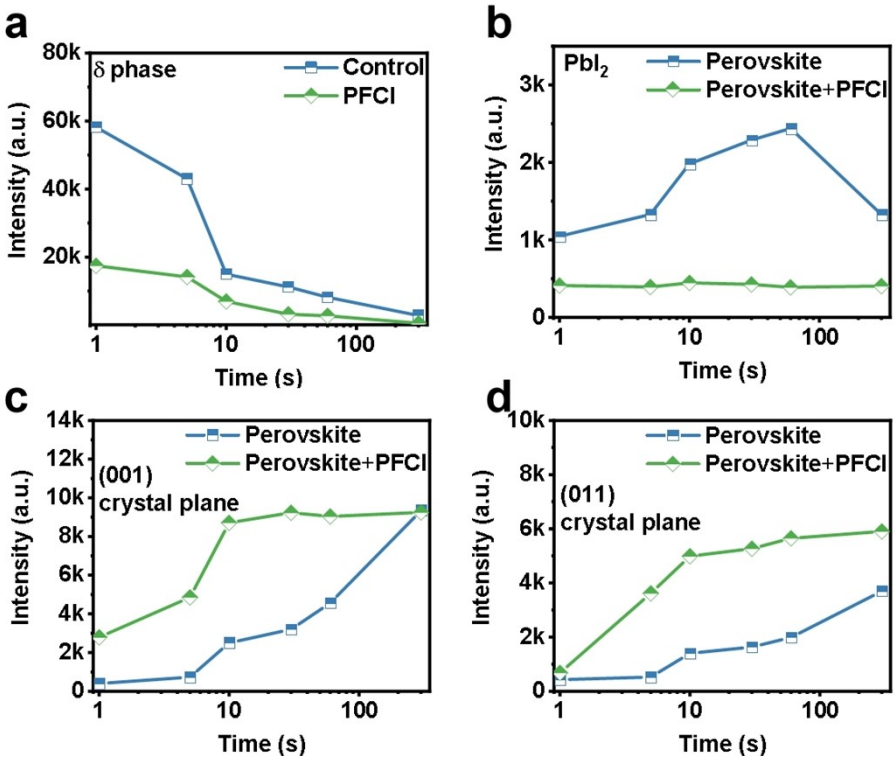

Fig. S2. XRD intensity evolution for **a** δ phase at 2θ = 11.82°, **b** PbI_2 phase at 2θ = 12.69°, **c** (001) crystal plane at 2θ = 14.00° and **d** (011) crystal plane at 2θ = 19.82° during the annealing process.

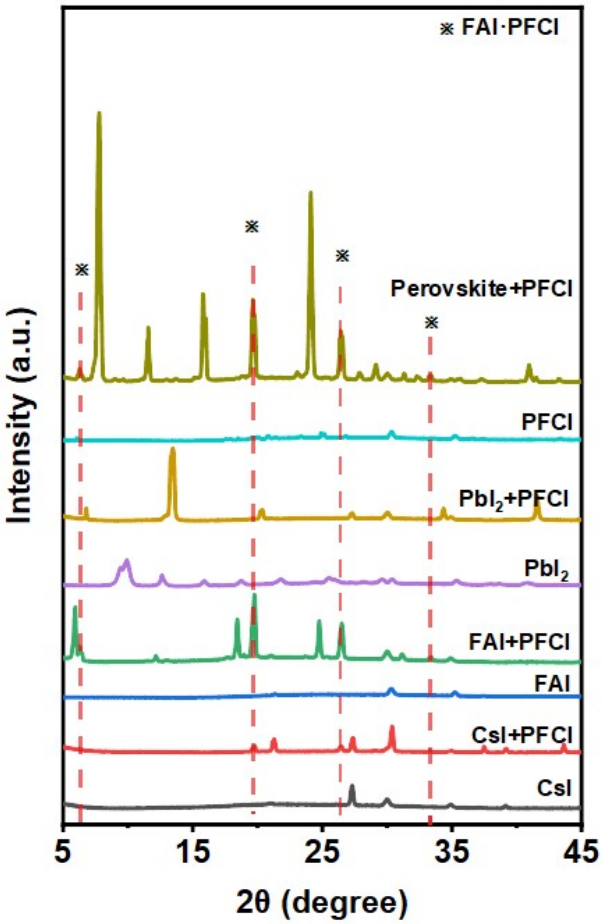

Fig. S3. XRD patterns of CsI, CsI+PFCl, FAI, FAI+PFCl, PbI_2, PbI_2+PFCl, PFCl and perovskite with PFCl films. For the films, the corresponding materials were dissolved in mixed solvents of DMF and DMSO (v/v, 4/1). The corresponding precursor solution was spin-coated on glass substrate at 2000 rpm for 10 s and then at 4000 rpm for 40 s and the wet films were not annealed. It needs to be pointed out that no anti-solvent was dripped during spin-coating.

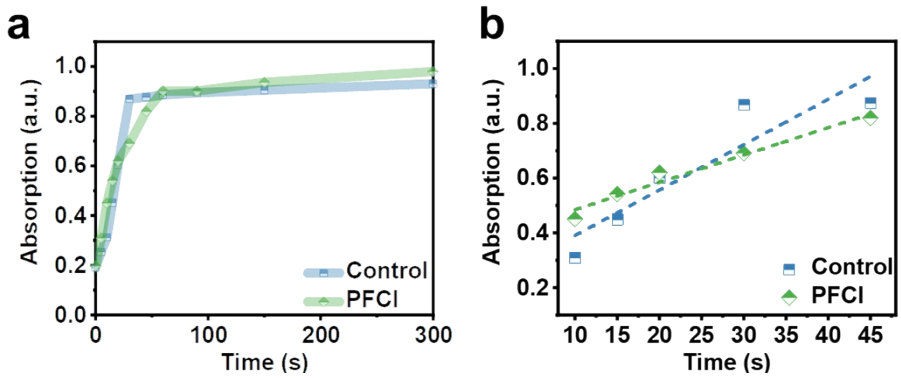

Fig. S4. **a** UV–vis absorption intensity evolution at the wavelength of 780 nm during the annealing. **b** Corresponding growth rates during annealing from 10 to 45 s.

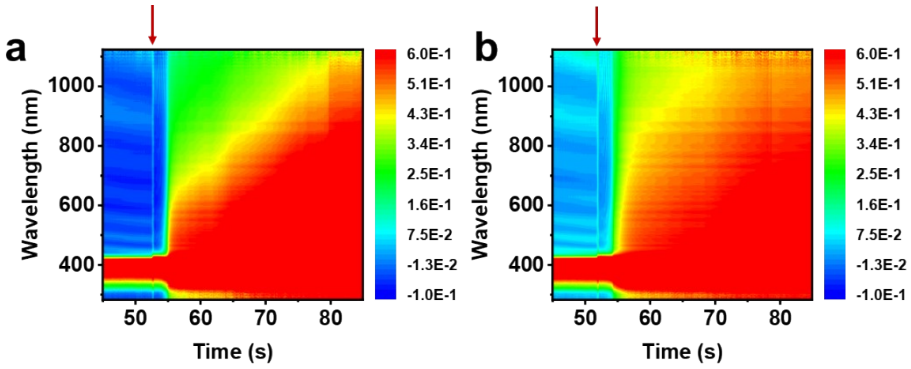

Fig. S5. The in-situ absorption spectra during spinning processes for the control and target perovskite intermediate films. Arrow indicates the antisolvent dropping.

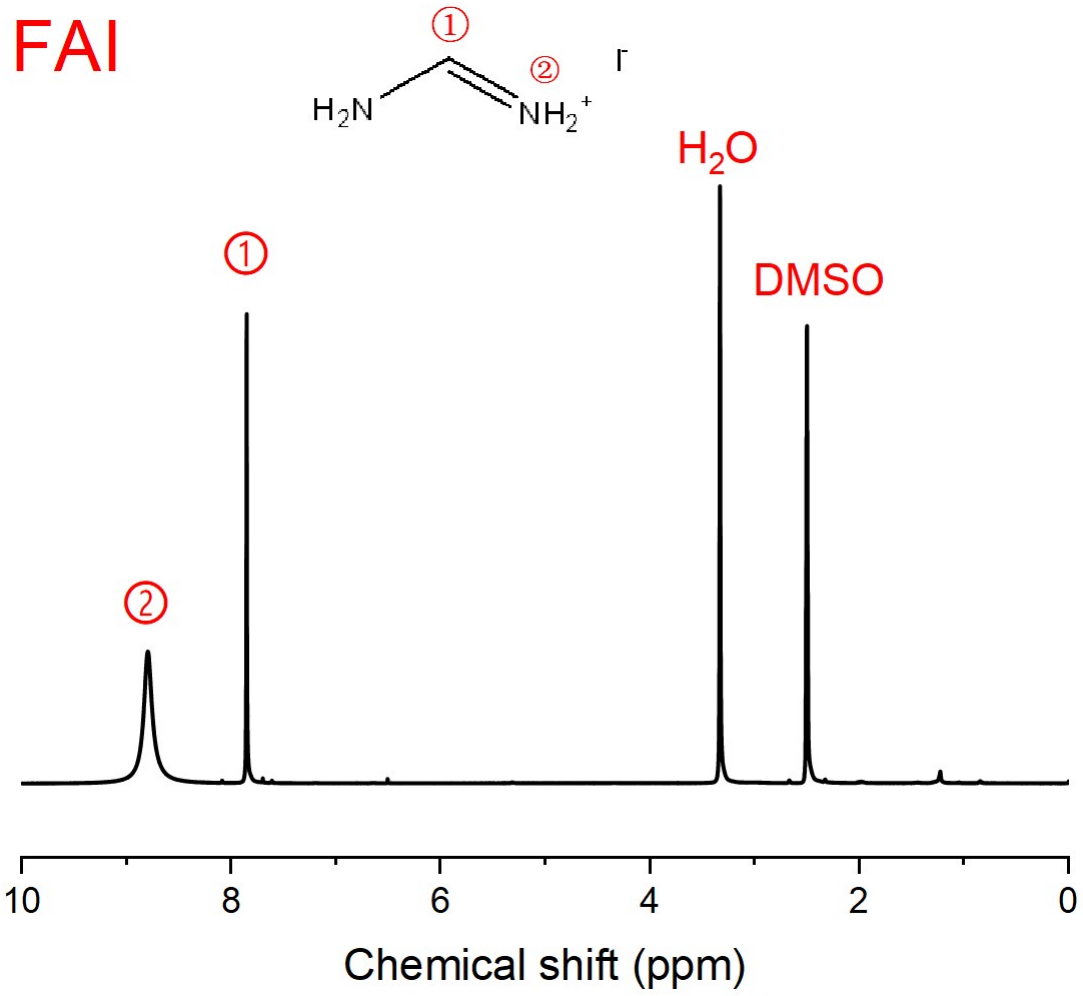

Fig. S6. ^{1}H NMR spectrum of FAI in DMSO-d6.

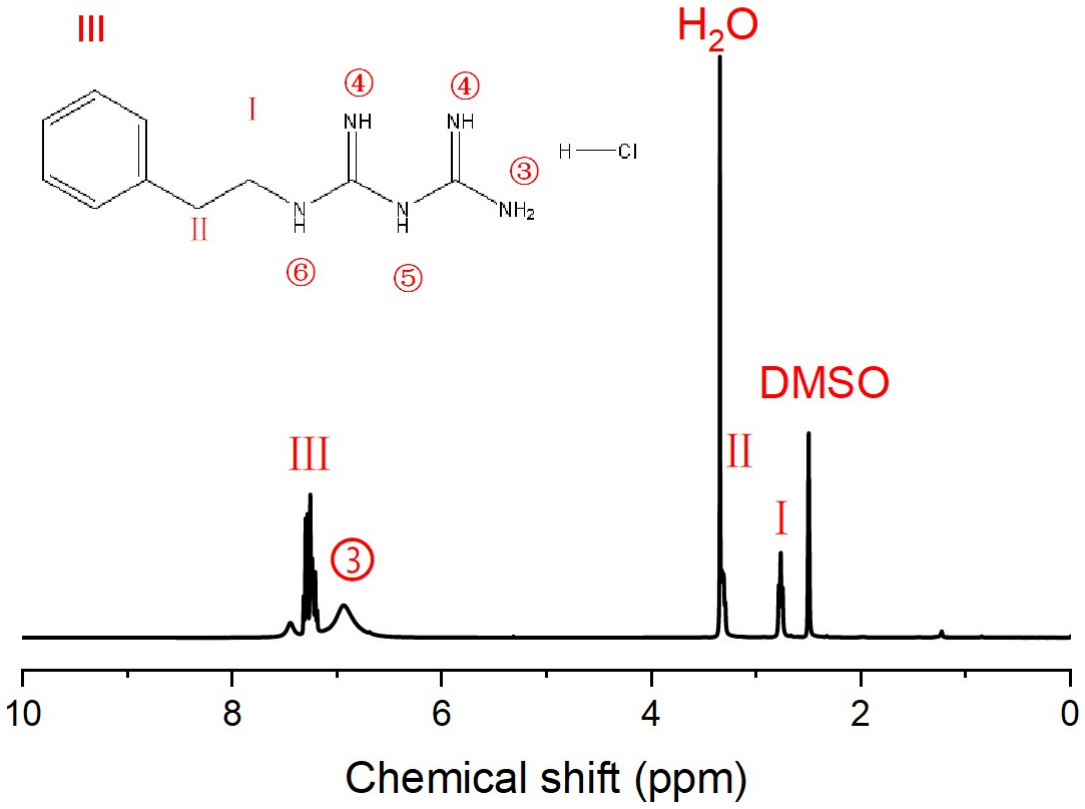

Fig. S7. ^{1}H NMR spectrum of PFCl in DMSO-d6.

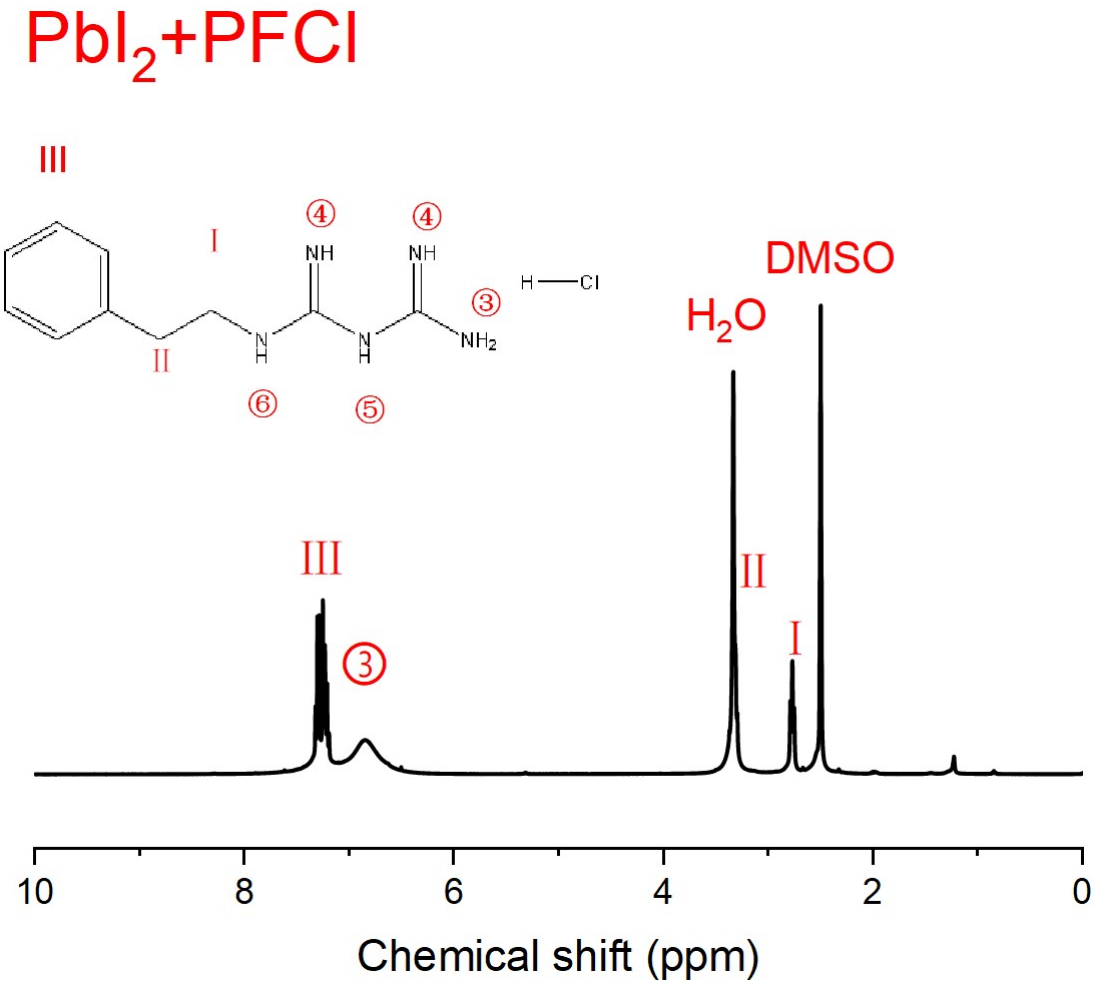

Fig. S8. ^{1}H NMR spectrum of PbI_2 (0.02M) and PFCI (0.02M) in DMSO-d6.

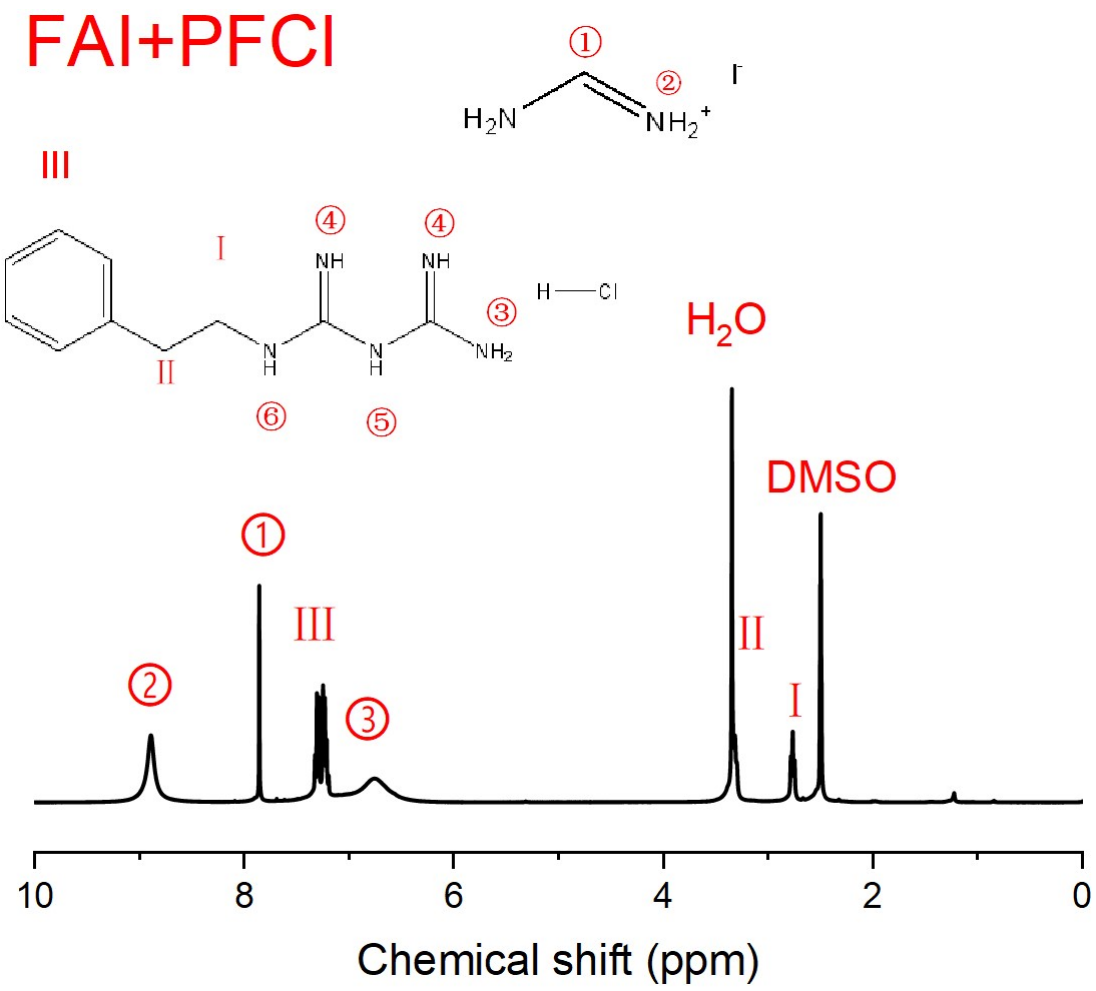

Fig. S9. ^{1}H NMR spectrum of FAI (0.02M) and PFCl (0.02M) in DMSO-d6.

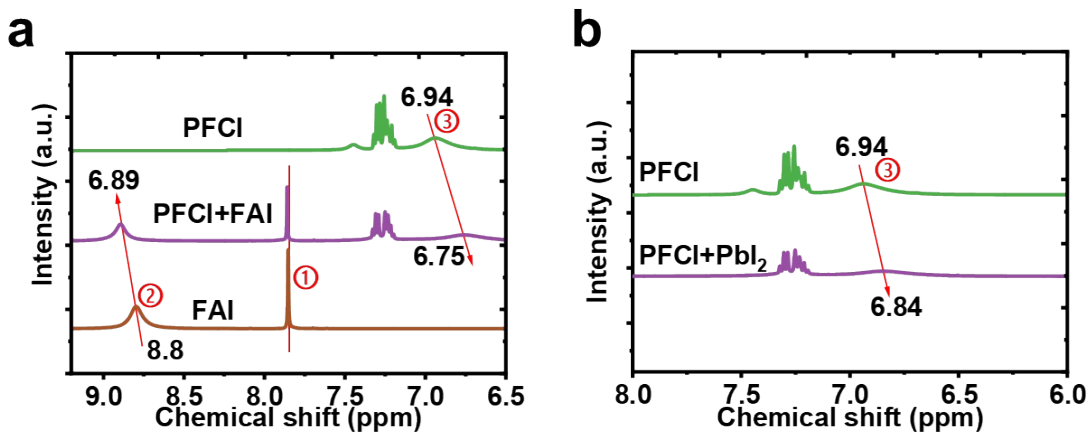

Fig. S10. a ^{1}H NMR spectra of PFCl (0.02M), FAI (0.02M), and FAI (0.02M) + PFCl (0.02M) in DMSO-d6. **b** ^{1}H NMR spectra of PFCl (0.02M) and PbI_2 (0.02M) + PFCl (0.02M) in DMSO-d6.

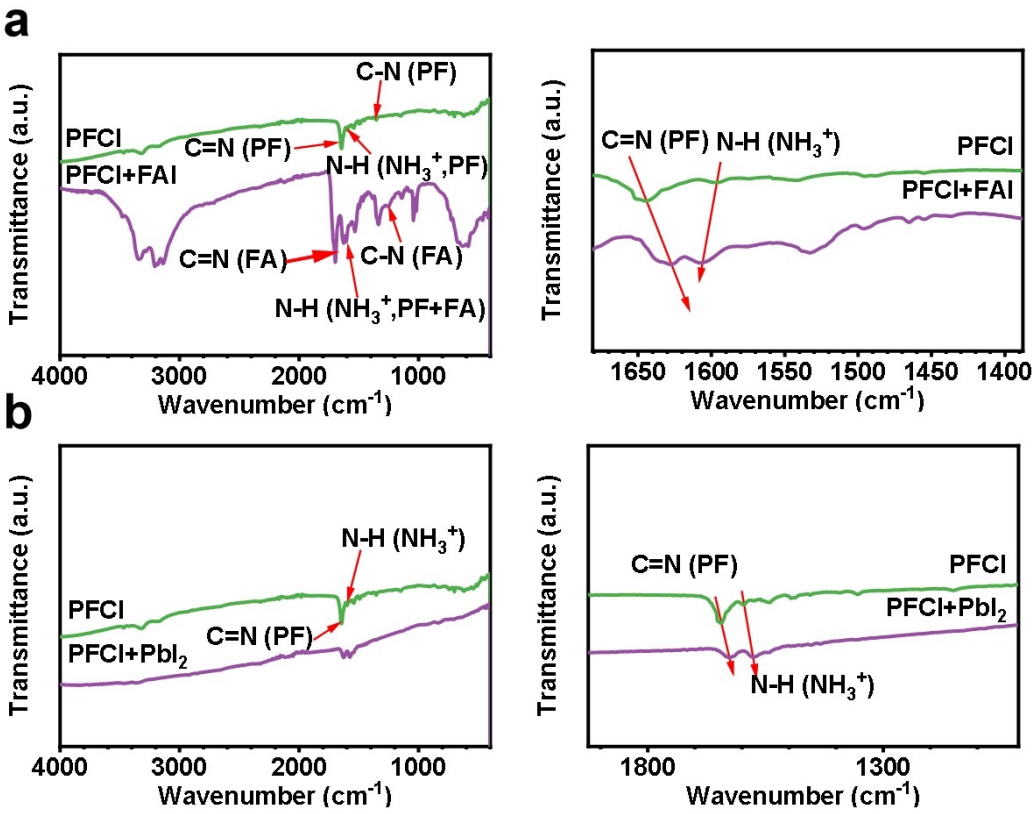

Fig. S11. **a** FTIR spectra of PFCl and PFCl+FAI films. **b** FTIR spectra of PFCl and PFCl+PbI_2 films.

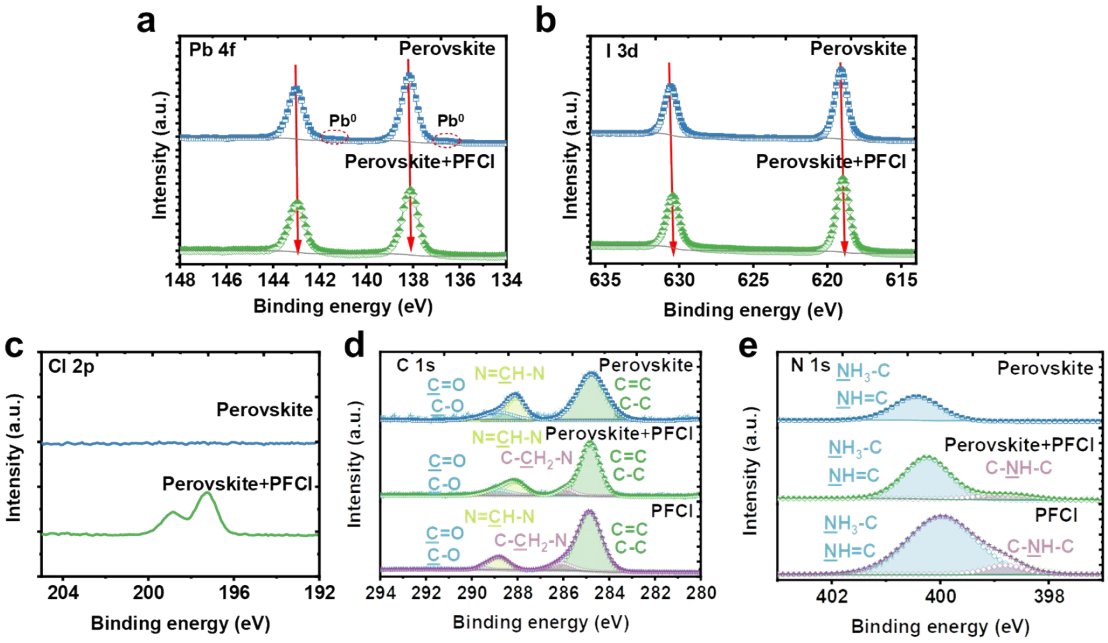

Fig. S12. XPS spectra of **a** Pb 4f, **b** I 3d and c Cl 2p for the perovskite films without and with PFCl. XPS of **d** C 1s and **e** N 1s for the perovskite, perovskite+PFCl and PFCl films.

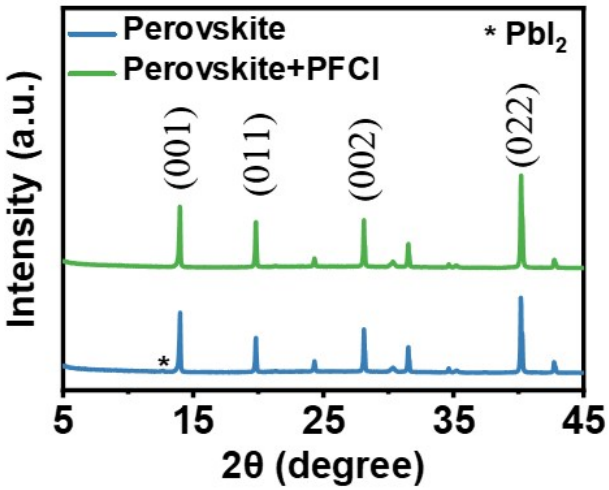

Fig. S13. XRD patterns of the perovskite films without and with PFCl after annealing at 100 ℃ for 30 min.

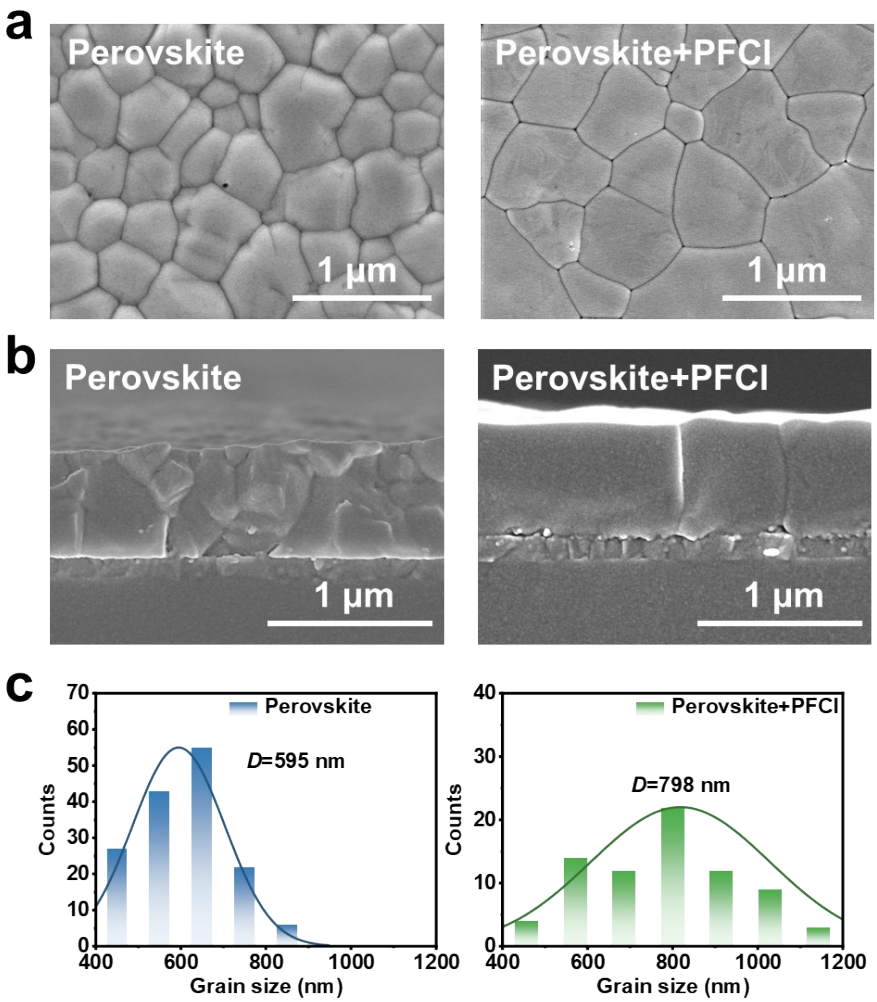

Fig. S14. Low-resolution **a** Top-view and **b** cross-sectional SEM images for the pristine and PFCl-modified perovskite films. **c** Statistic distribution histogram of the grain sizes (*D* represents the average grain size).

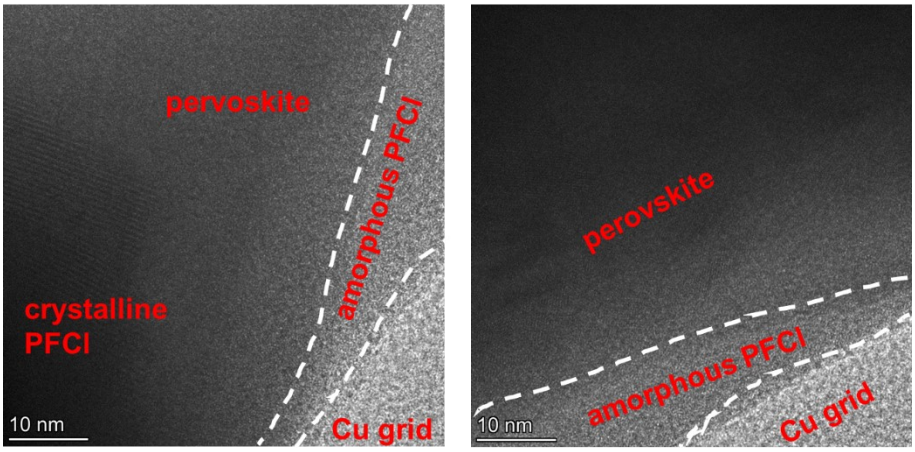

Fig. S15. TEM images of the PFCl-modified perovskite films.

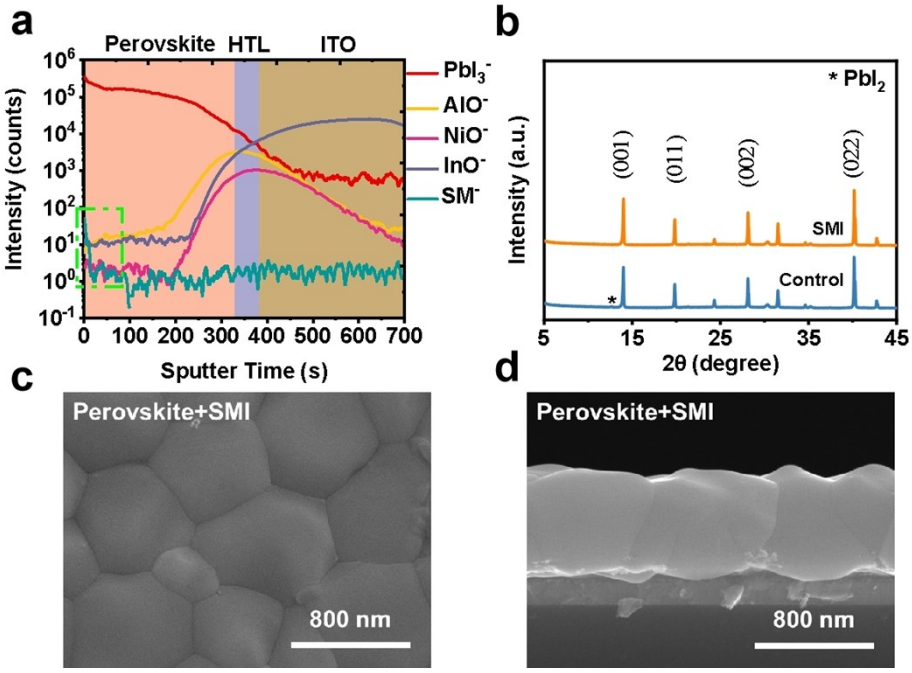

Fig. S16. a Spatial element distribution profile of SMI-modified device measured by ToF-SIMS. **b** XRD patterns for the perovskite films without and with SMI. **c** top-view and **d** cross-sectional SEM images for the SMI-modified perovskite films.

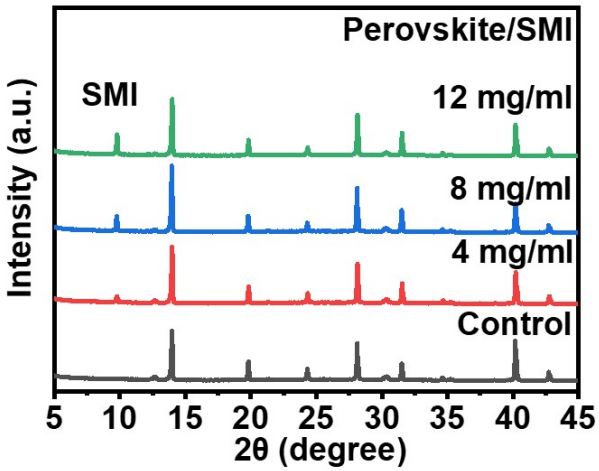

Fig. S17 XRD patterns for the perovskite films with different concentrations of SMI modified.

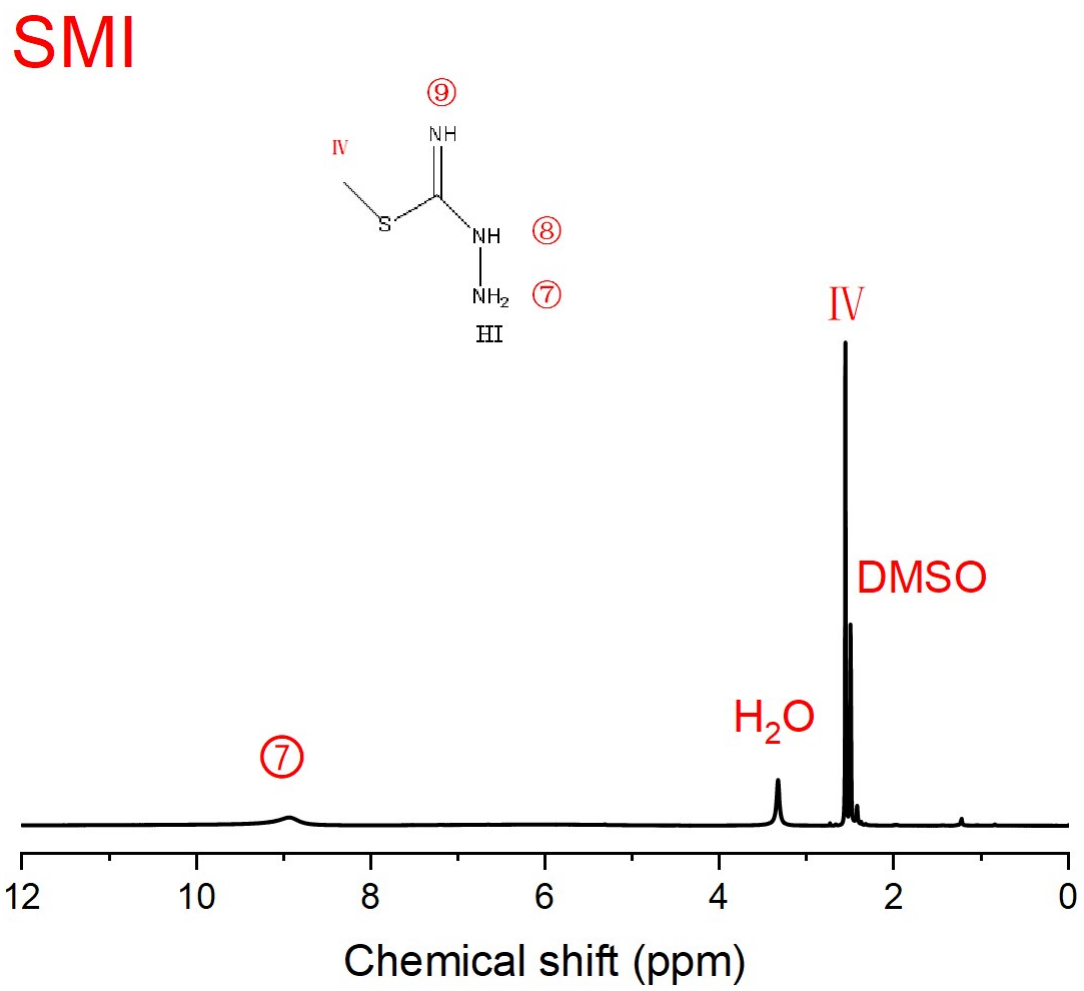

Fig. S18. ^{1}H NMR spectra of SMI in DMSO-d6.

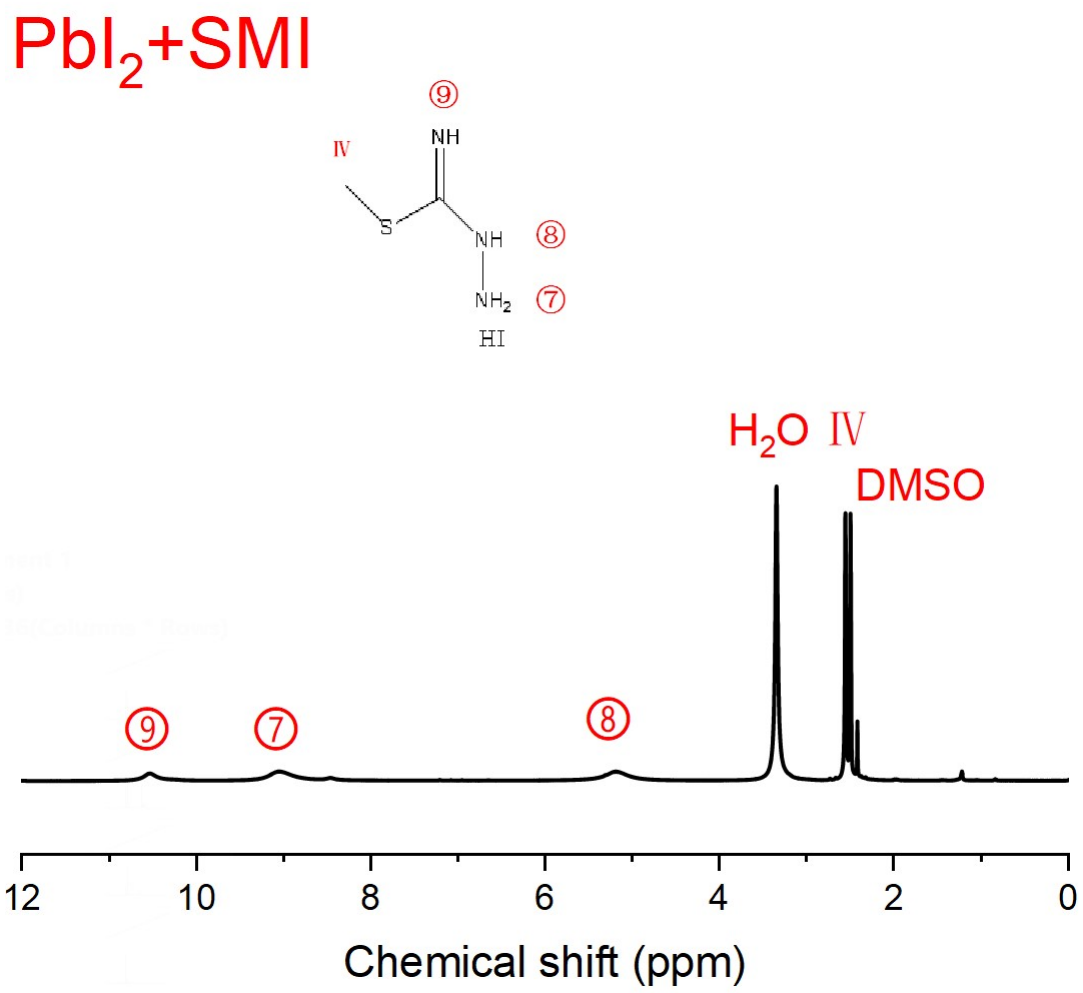

Fig. S19. ^{1}H NMR spectra of PbI_2 (0.02M) and SMI (0.02M) in DMSO-d6.

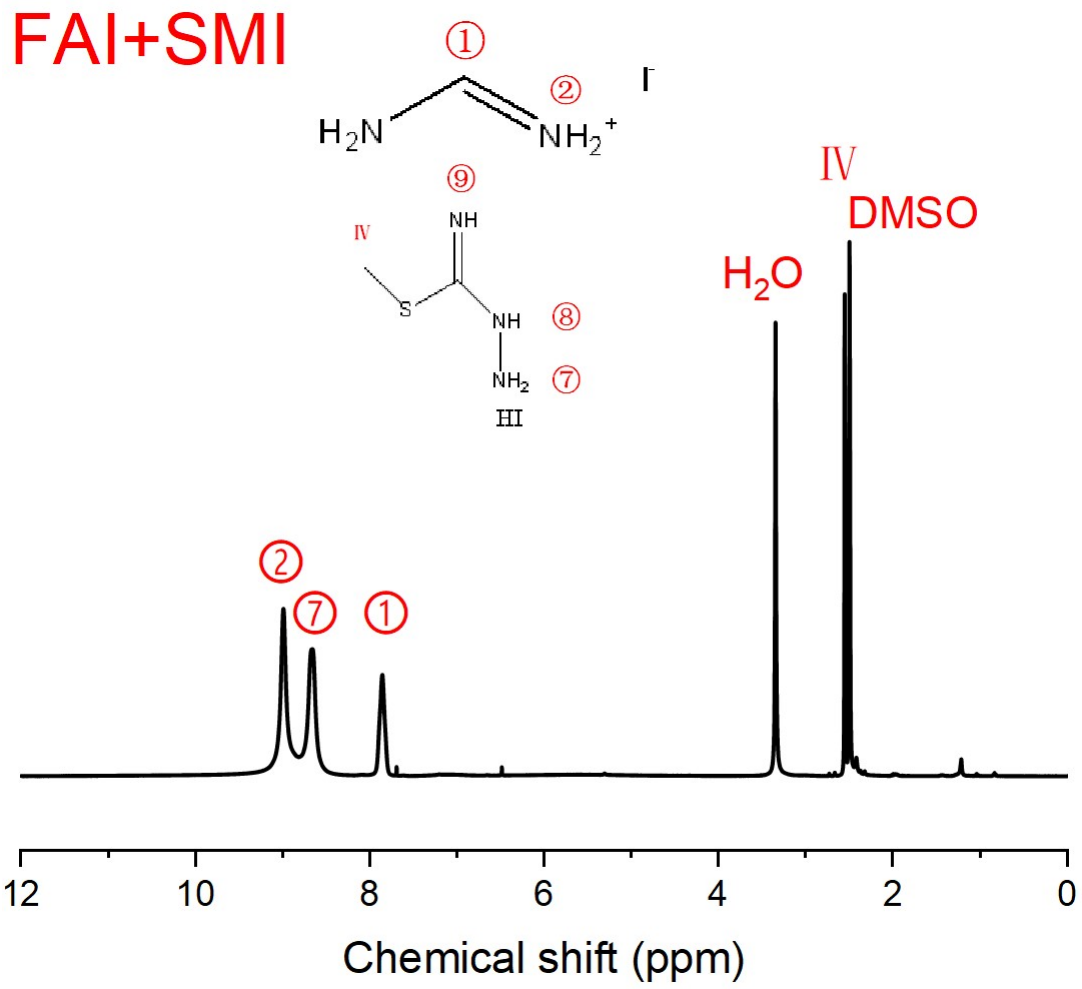

Fig. S20. ^{1}H NMR spectra of FAI (0.02M) and SMI (0.02M) in DMSO-d6.

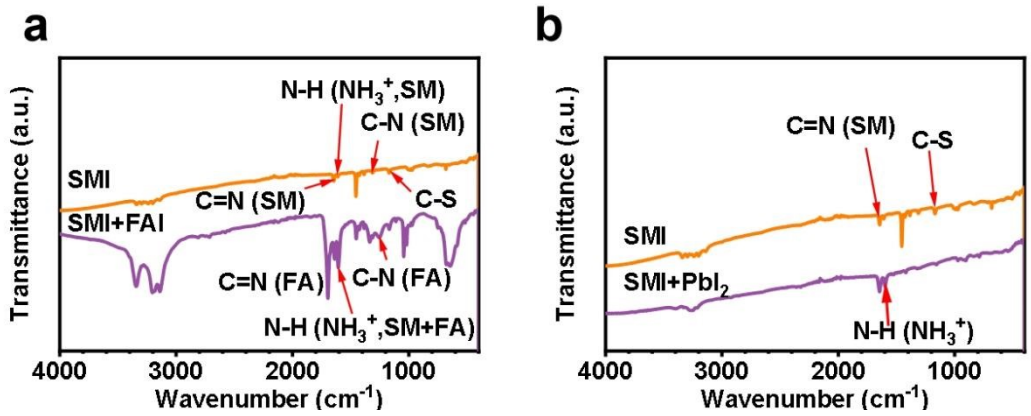

Fig. S21. FTIR spectra for **a** SMI and SMI+FAI films, and **b** SMI and SMI+PbI_2 films.

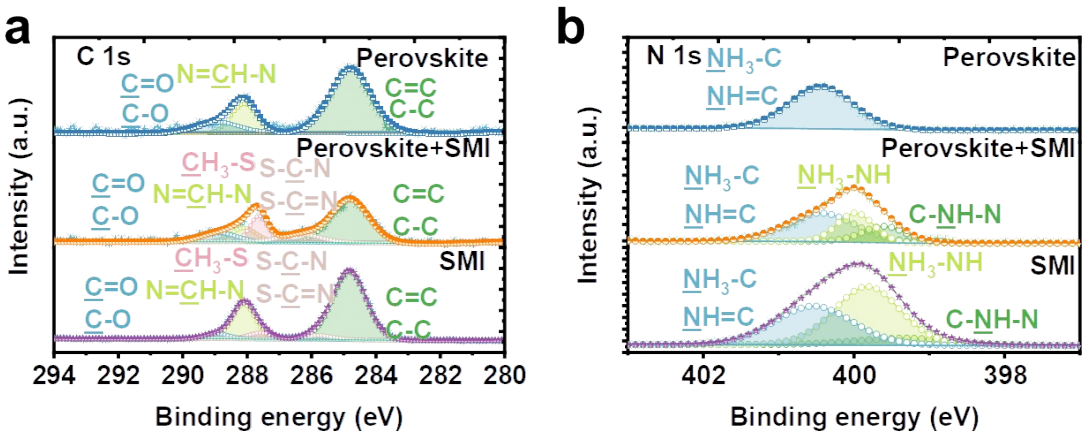

Fig. S22. XPS of **a** C 1s and **b** N 1s for the perovskite, perovskite/SMI and SMI films.

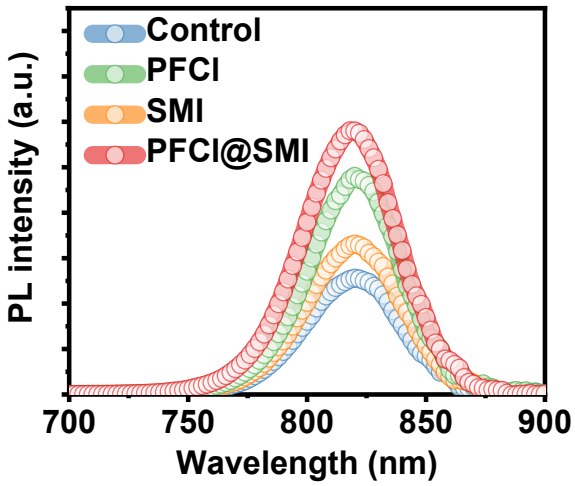

Fig. S23. Steady state PL spectra of the perovskite films on glass substrates.

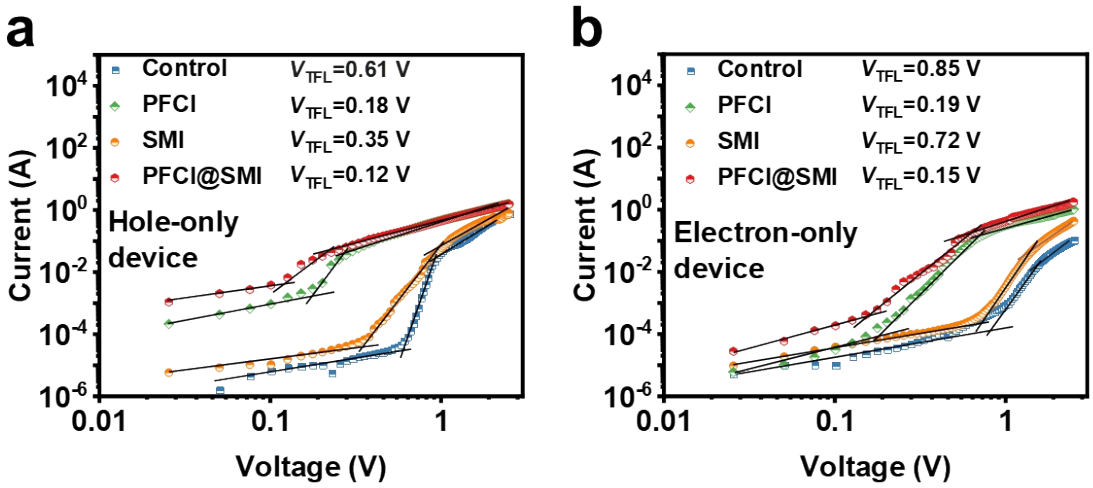

Fig. S24. Dark *I–V* curves for the **a** hole-only devices and **b** electron-only devices. The structure of hole-only device is ITO/NiO_x/perovskite without or with modifier/Spiro-OMeTAD/Ag. The structure of electron-only devices is ITO/SnO_2/perovskite without or with modifier/PCBM/Ag.

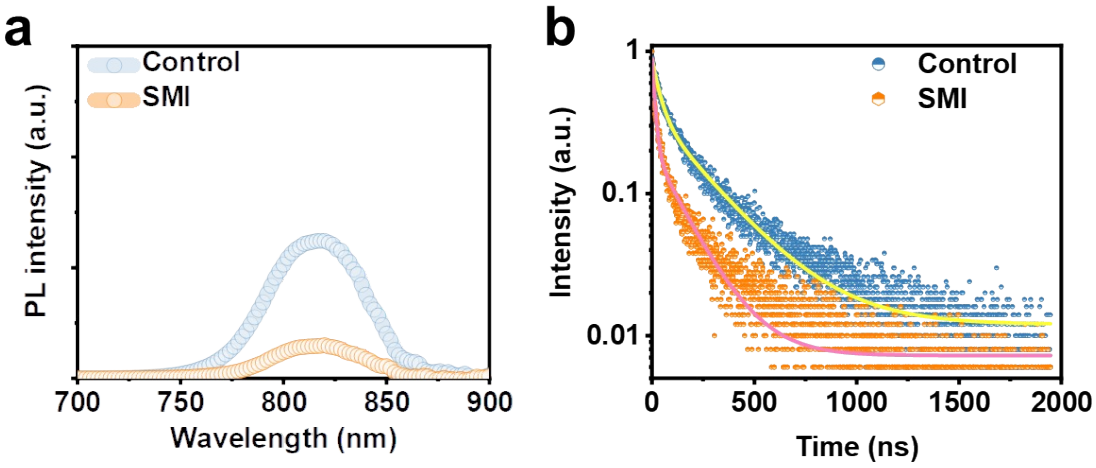

Fig. S25. a Steady state PL spectra and **b** TRPL of glass/perovskite/PCBM and glass/perovskite/SMI/PCBM films.

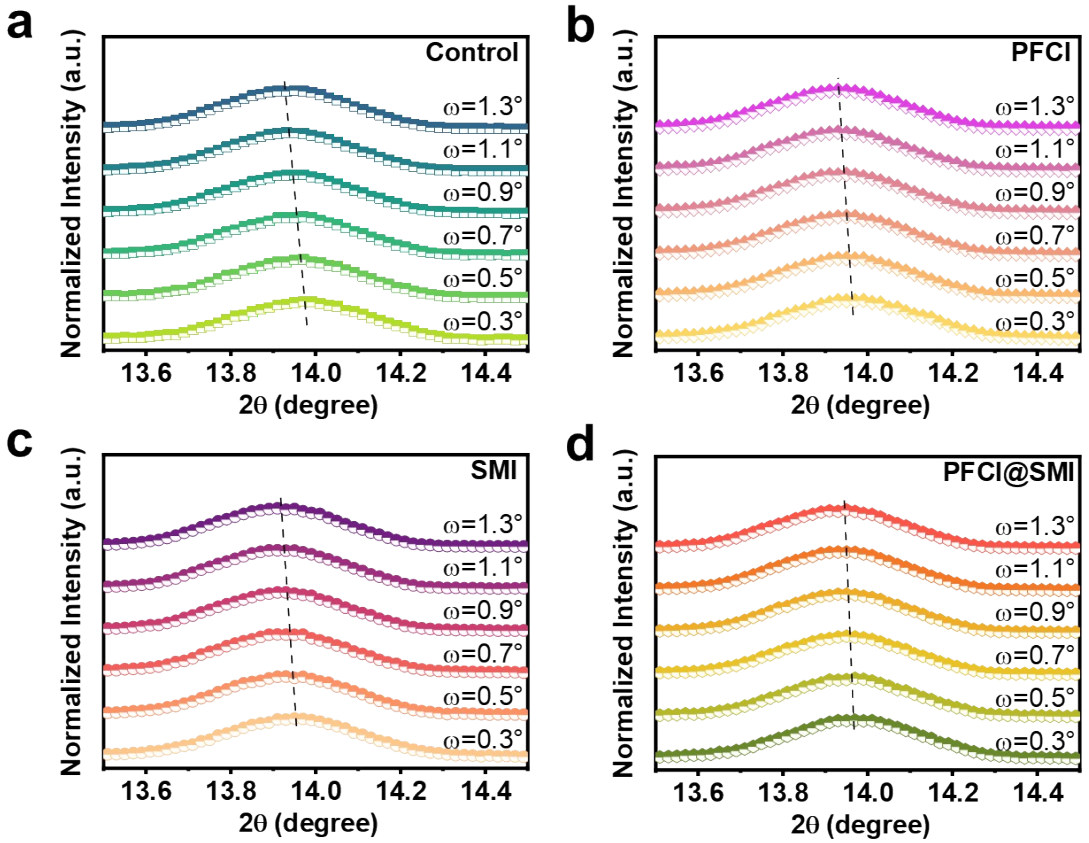

Fig. S26. GIXRD patterns with different ω values (0.3–1.3) for **a** control, **b** PFCl-, **c** SMI-, and **d** PFCl@SMI-modified perovskite films.

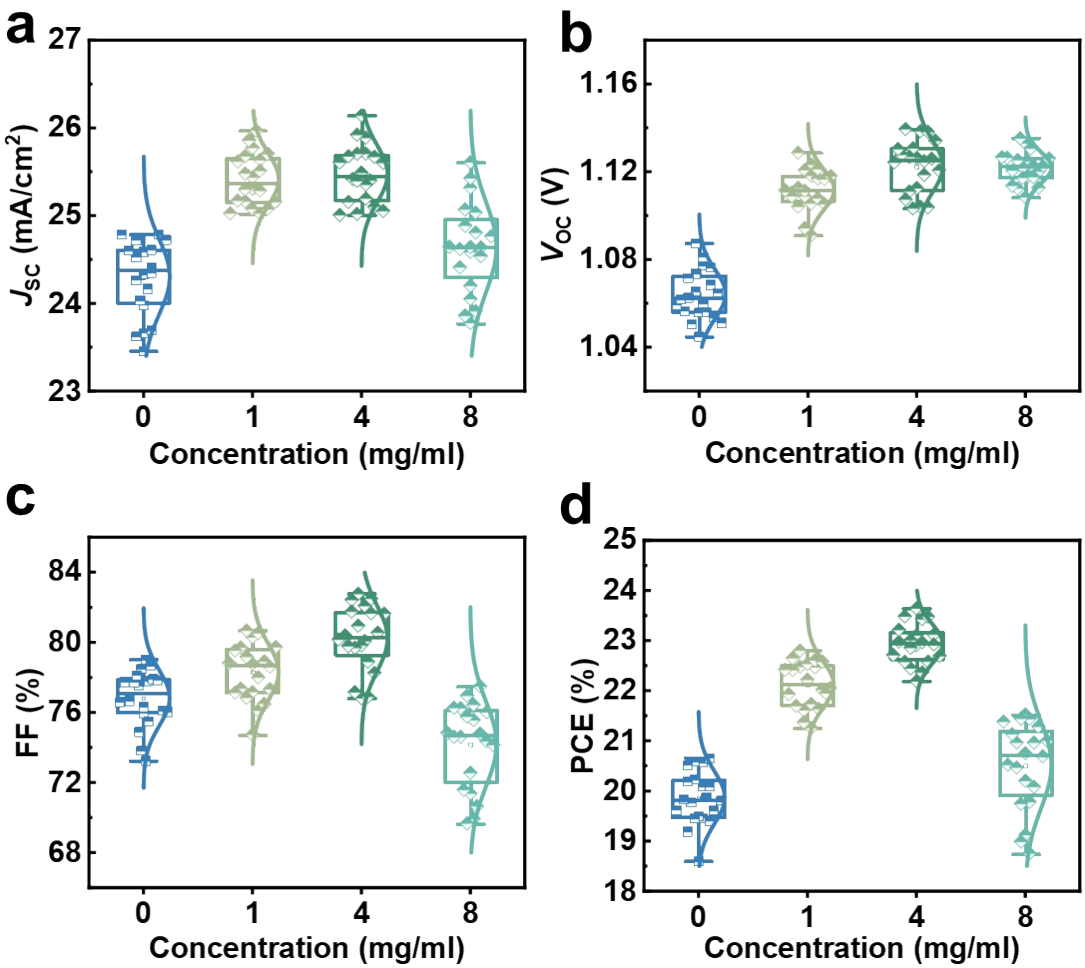

Fig. S27. a J_{SC}, **b** V_{OC}, **c** FF, and **d** PCE statistical diagrams of the devices with different concentrations of PFCl.

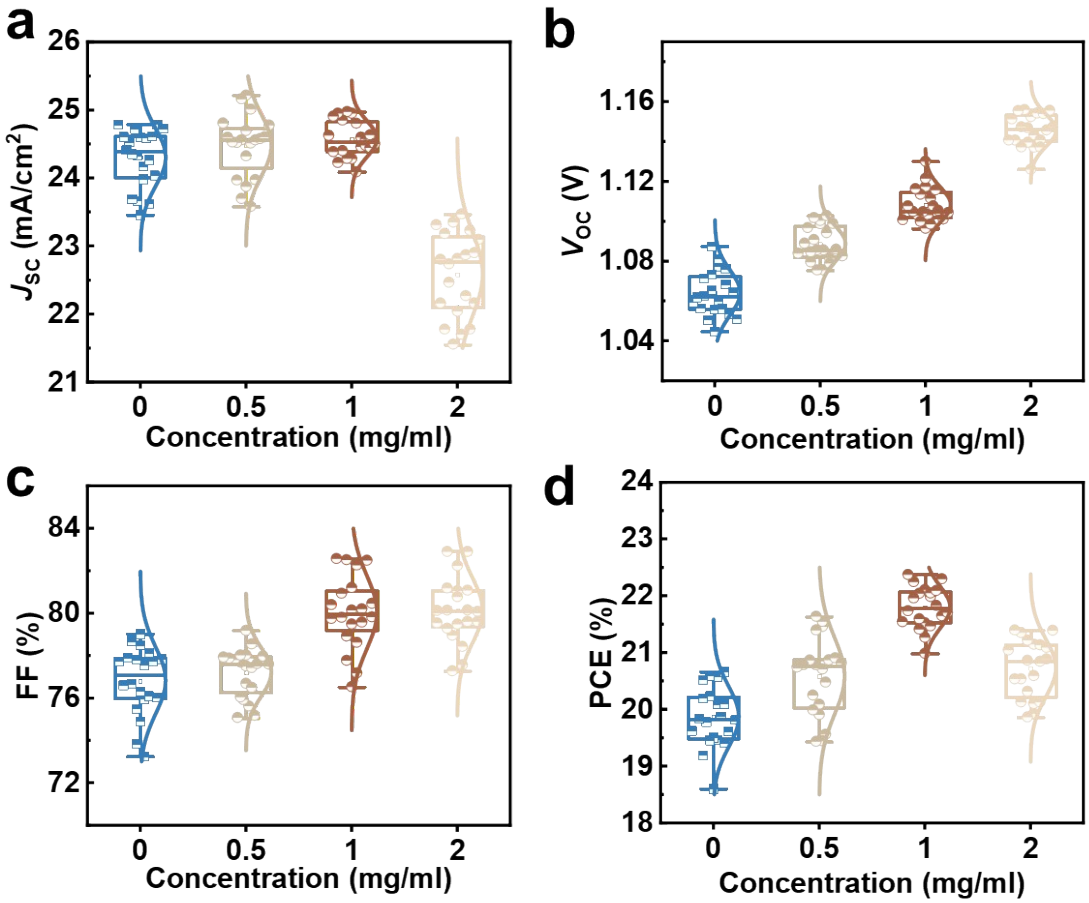

Fig. S28. a J_{SC}, **b** V_{OC}, **c** FF, and **d** PCE statistical diagrams of the devices with different concentrations of SMI.

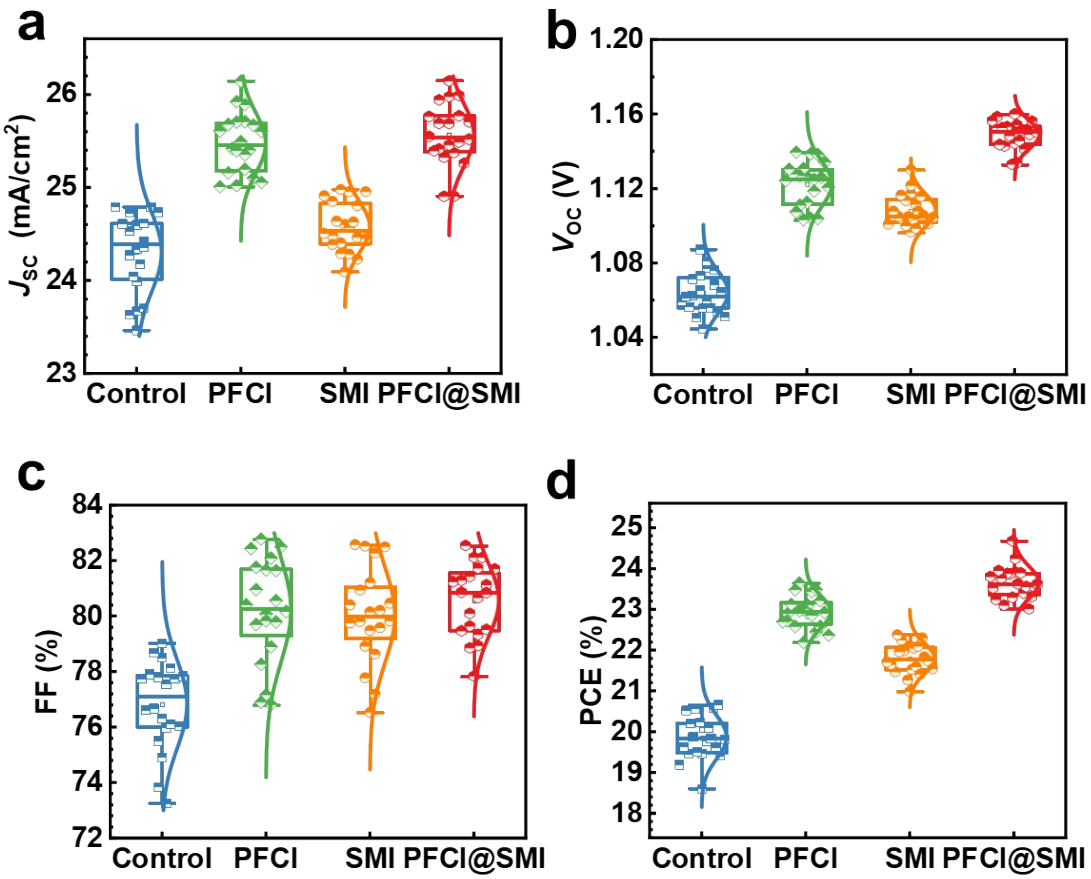

Fig. S29. a J_{SC}, **b** V_{OC}, **c** FF, and **d** PCE statistical diagrams for the control, PFCl-, SMI- and PFCl@SMI-modified devices (twenty samples for each condition).

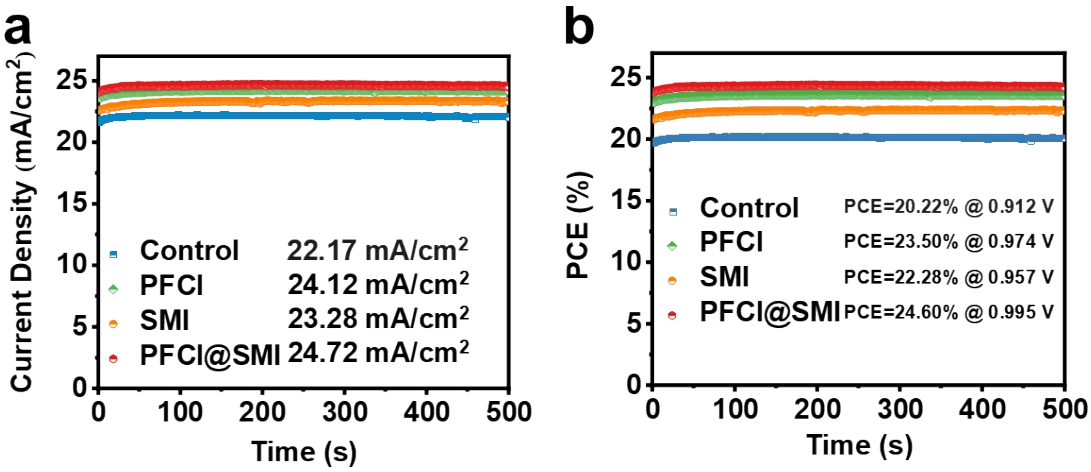

Fig. S30. a Current densities and **b** PCEs at MPP for the control and modified PSCs.

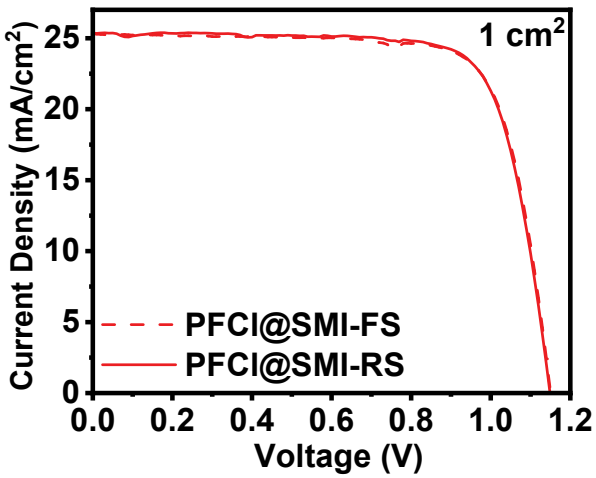

Fig. S31. *J-V* curves of large-area (1 cm^2) inverted PSCs with PFCl and SMI modification.

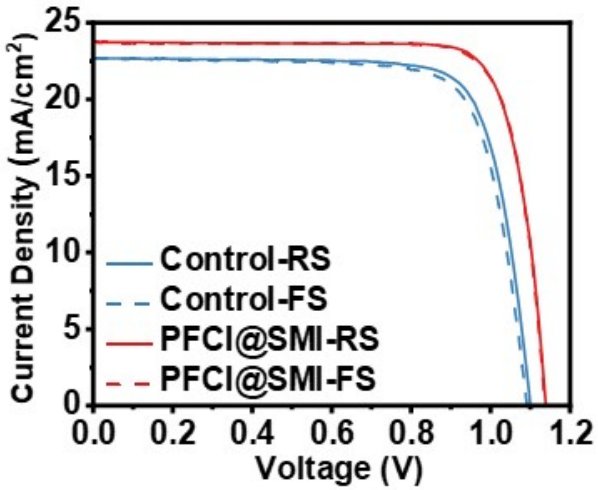

Fig. S32. *J-V* curves of the $(FA_{0.85}MA_{0.15})_{0.95}Cs_{0.05}Pb(I_{0.85}Br_{0.15})_3$-based PSCs without (control) and with synergistic modification.

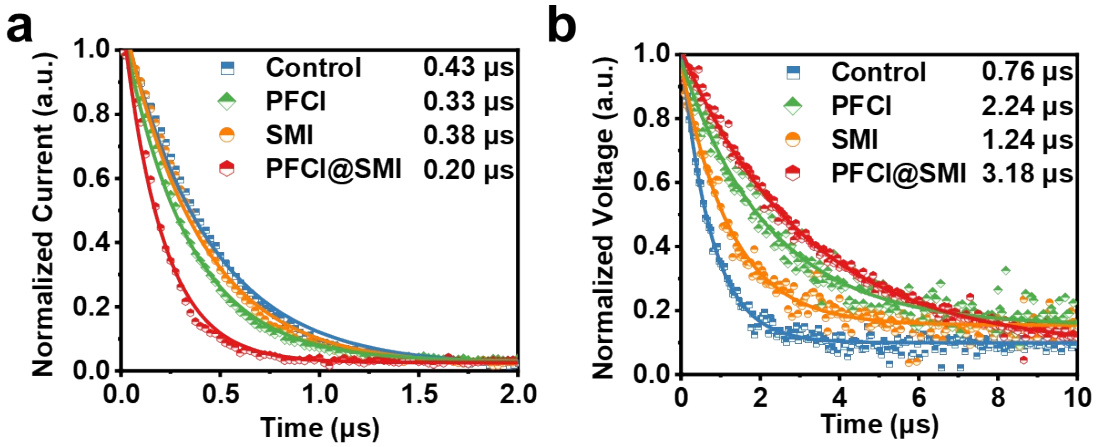

Fig. S33. a TPC and **b** TPV of the PSCs.

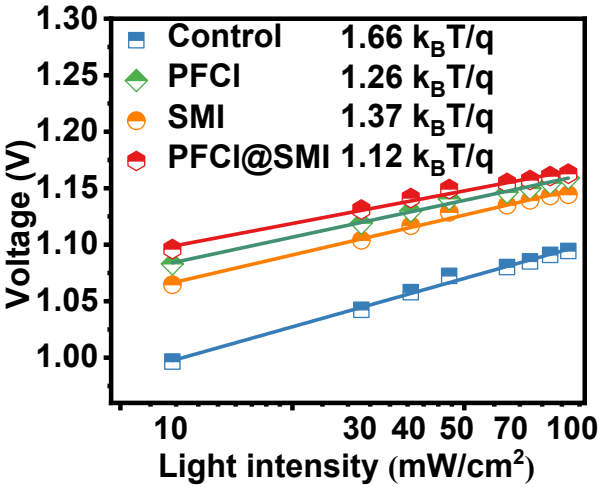

Fig. S34. Light-intensity-dependent V_{OC}. q is electron charge. k_B is Boltzmann constant. T is kelvin temperature.

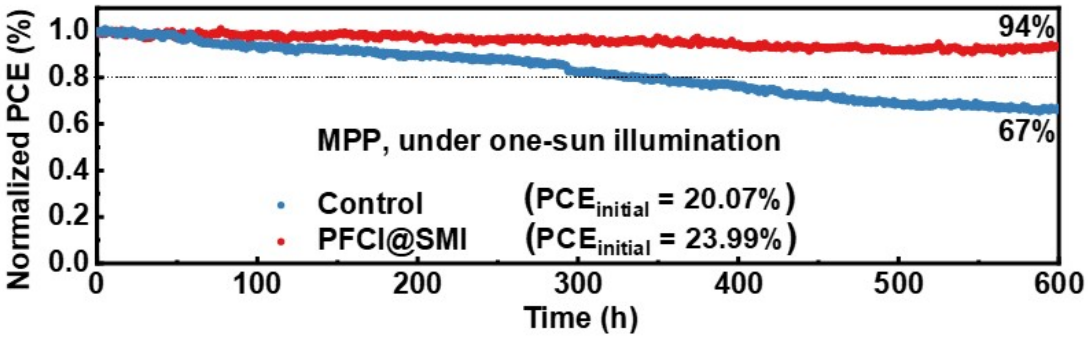

Fig. S35. Stability evolution of unencapsulated control and target devices measured at maximum power point under continuous one-sun illumination in N_2.

Table S1. Fitted results of TRPL curves of the control and modified perovskite films deposited on glass substrates.

Samples	Control	SMI	PFCl	PFCl@SMI
A_1(%)	66.74	68.17	72.28	84.45
τ_1(ns)	110.35	117.4	122.16	143.79
A_2(%)	33.26	31.83	27.72	15.55
τ_2(ns)	535.25	597.45	695.2	1731.75
τ_{ave}(ns)	251.69	270.19	280.98	390.76

TRPL spectra were fitted by using the double exponential function equation of $I(t) = I_0 + A_1\exp(-t/\tau_1) + A_2\exp(-t/\tau_2)$, where A_1 and A_2 represent the decay amplitude of fast and slow decay process, respectively. τ_1 and τ_2 stand for the fast and slow decay time constants, respectively. The average carrier lifetime (τ_{ave}) was calculated through the equation of $\tau_{ave} = (A_1\tau_1^2 + A_2\tau_2^2)/(A_1\tau_1 + A_2\tau_2)$. PVSK stands for perovskite.

Table S2. Fitted results of glass/perovskite/PCBM and glass/perovskite/SMI/PCBM films.

Samples	Control	SMI
A_1(%)	52.01	68.78
τ_1(ns)	38.11	14.54
A_2(%)	47.99	31.22
τ_2(ns)	249.61	150.21
τ_{ave}(ns)	139.61	56.9

Table S3. Photovoltaic parameters of the PSCs based on different concentrations of PFCl in the range of 1 to 8 mg/mL. *J–V* curves were measured with a scan rate of 100 mV/s under AM 1.5G illumination.

Concentration (mg/mL)		J_{SC} (mA/cm^2)	V_{OC} (V)	FF (%)	PCE (%)
0	Average	24.3±0.42	1.064±0.011	76.83±1.58	19.87±0.53
	Champion	24.61	1.077	77.76	20.60
1	Average	25.41±0.3	1.112±0.009	78.3±1.61	22.12±0.46
	Champion	25.70	1.118	78.82	22.65
4	Average	25.46±0.3	1.123±0.013	79.98±2.21	22.87±0.41
	Champion	25.71	1.126	81.67	23.65
8	Average	24.64±0.51	1.122±0.007	74.2±2.4	20.52±0.86
	Champion	25.04	1.125	76.45	21.53

Table S4. Photovoltaic parameters of the PSCs based on different concentrations of SMI in the range of 0.5 to 2 mg/mL. *J–V* curves were measured with a scan rate of 100 mV/s under AM 1.5G illumination.

Concentration (mg/mL)		J_{SC} (mA/cm^2)	V_{OC} (V)	FF (%)	PCE (%)
0	Average	24.3±0.42	1.064±0.011	76.83±1.58	19.87±0.53
	Champion	24.79	1.060	78.69	20.67
0.5	Average	24.48±0.45	1.089±0.009	77.22±1.14	20.59±0.68
	Champion	24.78	1.103	79.19	21.64
1	Average	24.57±0.26	1.108±0.009	80.04±1.71	21.8±0.37
	Champion	24.49	1.108	82.50	22.38
2	Average	22.59±0.61	1.146±0.008	80.13±1.52	20.73±0.51
	Champion	23.19	1.151	80.16	21.40

Table S5. Photovoltaic parameters of the PSCs based on different modification. *J–V* curves were measured with a scan rate of 100 mV/s under AM 1.5G illumination.

Devices		J_{SC} (mA/cm^2)	V_{OC} (V)	FF (%)	PCE (%)
Control	Average	24.3±0.42	1.064±0.011	76.83±1.58	19.87±0.53
	Champion	24.79	1.060	78.69	20.67
PFCl	Average	25.69±0.36	1.13±0.007	79.23±1.99	22.99±0.45
	Champion	25.71	1.126	81.67	23.65
SMI	Average	24.57±0.26	1.108±0.009	80.04±1.71	21.8±0.37
	Champion	24.49	1.108	82.50	22.38
PFCl@SMI	Average	25.57±0.35	1.149±0.007	80.54±1.26	23.66±0.39
	Champion	25.99	1.156	82.11	24.67

Table S6. Comparison of the photovoltaic performance of the inverted PSCs in this work with the literatures which reported PCEs over 23%.

Device structure	V_{oc} (V)	J_{sc} (mA/cm^2)	FF (%)	PCE (%)	Ref.
ITO/PTAA/$(Cs_{0.15}FA_{0.85})Pb(I_{0.95}Br_{0.05})_3$/ PCBM/BCP/Ag	1.150	24.61	82.1	23.10	[2]
ITO/MeO-2PACz/$FA_{0.88}Cs_{0.12}PbI_{2.64}Br_{0.36}$/ PCBM/BCP/Ag	1.164	23.19	85.7	23.13	[3]
ITO/NiO_x/PTAA/Al_2O_3/$FA_{0.95}Cs_{0.05}PbI_3$/ PCBM/BCP/Ag	1.138	25.38	81.4	23.49	[4]
ITO/P3CT-N/$Cs_{0.05}FA_{0.95}PbI_3$/C_{60}/TPBi/Cu	1.140	26.30	78.6	23.50	[5]
ITO/NiOx/$Cs_{0.05}MA_{0.1}FA_{0.85}PbI_3$/ quasi-2D/PCBM/BCP/Ag	1.16	24.4	82.5	23.3	[6]
ITO/2PACz/3D perovskite/ 2D-RT/ C60/BCP/Ag	1.2	-	82	24.3	[7]
ITO/PTAA/$Cs_{0.05}(FA_{0.98}MA_{0.02})_{0.95}Pb(I_{0.98}Br_{0.02})_3$/ C_{60}/BCP/Ag	1.179	25.59	80.6	24.5	[8]
ITO/MeO-2PACZ/$Rb_{0.05}Cs_{0.05}MA_{0.05}FA_{0.85}Pb(I_{0.95}Br_{0.05})_3$/(LiF)/C60/BCP/Ag	1.15	26.13	84.6	25.49	[9]
ITO/NiO_x/PTAA/Al_2O_3/$Cs_{0.05}FA_{0.95}PbI_3$/ PCBM/BCP/Ag	**1.156**	**25.99**	**82.11**	**24.67**	**This work**

Table S7. PV parameters of the large-area (1 cm^2) inverted PSCs with PFCl and SMI modification.

Scan direction	J_{SC} (mA/cm^2)	V_{OC} (V)	FF (%)	PCE (%)
Reverse	25.32	1.151	77.12	22. 48
Forward	25.24	1.149	76.44	22.16

Table S8. PV parameters of the $(FA_{0.85}MA_{0.15})_{0.95}Cs_{0.05}Pb(I_{0.85}Br_{0.15})_3$-based PSCs without (control) and with synergistic modification.

Devices	Scan direction	J_{SC} (mA/cm^2)	V_{OC} (V)	FF (%)	PCE (%)
Control	Reverse	22.70	1.100	77.75	19.41
	Forward	22.68	1.091	76.43	18.91
PFCl@SMI	Reverse	23.77	1.138	81.82	22.14
	Forward	23.71	1.136	81.84	22.04

Supplementary references

1. H. Zhang, J. Cheng, F. Lin, H. He, J. Mao, K. S. Wong, A. K. Y. Jen and W. C. H. Choy, *ACS Nano*, 2016, **10**, 1503–1511.
2. S. Liu, X. Guan, W. Xiao, R. Chen, J. Zhou, F. Ren, J. Wang, W. Chen, S. Li, L. Qiu, Y. Zhao, Z. Liu and W. Chen, *Adv. Funct. Mater.*, 2022, **32**, 2205009.
3. L. Xie, X. Zhao, J. Wang, J. Li, C. Liu, S. Wang, Q. Bao, M. Yang, X. Niu, F. Hao and Z. Ge, *InfoMat*, 2022, **5**, e12379.
4. M. Li, H. Li, Q. Zhuang, D. He, B. Liu, C. Chen, B. Zhang, T. Pauporté, Z. Zang and J. Chen, *Angew. Chem. Int. Ed.*, 2022, **61**, e202206914.
5. X. Li, W. Zhang, X. Guo, C. Lu, J. Wei and J. Fang, *Science*, 2022, **375**, 434–437.
6. H. Chen, S. Teale, B. Chen, Y. Hou, L. Grater, T. Zhu, K. Bertens, S. M. Park, H. R. Atapattu, Y. Gao, M. Wei, A. K. Johnston, Q. Zhou, K. Xu, D. Yu, C. Han, T. Cui, E. H. Jung, C. Zhou, W. Zhou, A. H. Proppe, S. Hoogland, F. Laquai, T. Filleter, K. R. Graham, Z. Ning and E. H. Sargent, *Nat. Photonics*, 2022, **16**, 352–358.
7. R. Azmi, E. Ugur, A. Seitkhan, F. Aljamaan, A. S. Subbiah, J. Liu, G. T. Harrison, M. I. Nugraha, M. K. Eswaran, M. Babics, Y. Chen, F. Xu, T. G. Allen, A. u. Rehman, C.-L. Wang, T. D. Anthopoulos, U. Schwingenschlögl, M. De Bastiani, E. Aydin and S. De Wolf, *Science*, 2022, **376**, 73–77.
8. Z. Li, B. Li, X. Wu, S. A. Sheppard, S. Zhang, D. Gao, N. J. Long and Z. Zhu, *Science*, 2022, **376**, 416–420.
9. Q. Jiang, J. Tong, Y. Xian, R. A. Kerner, S. P. Dunfield, C. Xiao, R. A. Scheidt, D. Kuciauskas, X. Wang, M. P. Hautzinger, R. Tirawat, M. C. Beard, D. P. Fenning, J. J. Berry, B. W. Larson, Y. Yan and K. Zhu, *Nature*, 2022, **611**, 278–283.